



1 **Impact of small-scale disturbances on geochemical conditions, biogeochemical processes**
2 **and element fluxes in surface sediments of the eastern Clarion-Clipperton Zone, Pacific**
3 **Ocean**

4 Jessica B. Volz^{a,*}, Laura Haffert^b, Matthias Haeckel^b, Andrea Koschinsky^c, Sabine Kasten^{a,d}

5 ^a Alfred Wegener Institute Helmholtz Centre for Polar and Marine Research, 27570
6 Bremerhaven, Germany

7 ^b GEOMAR Helmholtz Centre for Ocean Research Kiel, 24148 Kiel, Germany

8 ^c Jacobs University Bremen, Department of Physics and Earth Sciences, 28759 Bremen,
9 Germany

10 ^d University of Bremen, Faculty of Geosciences, Klagenfurter Strasse, 28359 Bremen, Germany

11

12 *Corresponding author:

13 Tel: +49 471 4831 1842

14 Email: Jessica.volz@awi.de

15

16

17

18 **Keywords:** Deep-sea mining, CCZ, polymetallic nodules, redox zonation, oxygen penetration
19 depth, solid-phase manganese

20



21 Abstract

22 The thriving interest in harvesting deep-sea mineral resources, such as polymetallic nodules,
23 calls for environmental impact studies, and ultimately, for regulations for environmental
24 protection. Industrial-scale deep-sea mining of polymetallic nodules most likely has severe
25 consequences for the natural environment. However, the effects of mining activities on deep-
26 sea ecosystems, sediment geochemistry and element fluxes are still poorly conceived.
27 Predicting the environmental impact is challenging due to the scarcity of environmental
28 baseline studies as well as the lack of mining trials with industrial mining equipment in the deep
29 sea. Thus, currently we have to rely on small-scale disturbances simulating deep-sea mining
30 activities as a first-order approximation to study the expected impacts on the abyssal
31 environment.

32 Here, we investigate surface sediments in disturbance tracks of seven small-scale benthic
33 impact experiments, which have been performed in four European contract areas for the
34 exploration of polymetallic nodules in the Clarion-Clipperton Zone (CCZ). These small-scale
35 disturbance experiments were performed 1 day to 37 years prior to our sampling program in the
36 German, Polish, Belgian and French contract areas using different disturbance devices. We
37 show that the depth distribution of solid-phase Mn in the upper 20 cm of the sediments in the
38 CCZ provides a reliable tool for the determination of the disturbance depth, which has been
39 proposed in a previous study (Paul et al., 2018). We found that the upper 5–15 cm of the
40 sediments were removed during various small-scale disturbance experiments in the different
41 exploration contract areas. Transient transport-reaction modelling for the Polish and German
42 contract areas reveals that the removal of the surface sediments is associated with the loss of
43 reactive labile organic carbon. As a result, oxygen consumption rates decrease significantly
44 after the removal of the surface sediments, and consequently, oxygen penetrates up to tenfold
45 deeper into the sediments inhibiting denitrification and Mn(IV) reduction. Our model results
46 show that the post-disturbance geochemical re-equilibration is controlled by diffusion until the
47 reactive labile TOC fraction in the surface sediments is partly re-established and the
48 biogeochemical processes commence. While the re-establishment of bioturbation is essential,
49 the geochemical re-equilibration of the sediments is ultimately controlled by the burial rates of
50 organic matter. Hence, under current depositional conditions, the new geochemical equilibrium
51 in the sediments of the CCZ is reached only on a millennia scale even for these small-scale
52 disturbances simulating deep-sea mining activities.

53



54 1. Introduction

55 The accelerating global demand for metals and rare-earth elements are driving the economic
 56 interest in deep-sea mining (e.g., Glasby, 2000; Hoagland et al., 2010; Wedding et al., 2015).
 57 Seafloor minerals of interest include (1) polymetallic nodules (e.g., Mero, 1965), (2) massive
 58 sulfide deposits (e.g., Scott, 1987) and (3) cobalt-rich crusts (e.g., Halkyard, 1985). As the
 59 seafloor within the Clarion-Clipperton Zone (CCZ) in the NE Pacific holds one of the most
 60 extensive deposits of polymetallic nodules with considerable base metal quantities, commercial
 61 exploitation of seafloor mineral deposits may focus on the CCZ (e.g., Mero, 1965; Halbach et
 62 al., 1988; Rühlemann et al., 2011; Hein et al., 2013; Kuhn et al., 2017a). The exploration, and
 63 ultimately, industrial exploitation of polymetallic nodules demands for international regulations
 64 for the protection of the environment (e.g., Halfar and Fujita, 2002; Glover and Smith, 2003;
 65 Davies et al., 2007; van Dover, 2011; Ramirez-Llodra et al., 2011; Boetius and Haeckel, 2018).
 66 The International Seabed Authority (ISA) is responsible for regulating the exploration and
 67 exploitation of marine mineral resources as well as for protecting and conserving the marine
 68 environment beyond the exclusive economic zones of littoral states from harmful effects (ISA,
 69 2010). The ISA has granted temporal contracts for the exploration of polymetallic nodules in
 70 the CCZ, engaging all contract holders to explore resources, test mining equipment and assess
 71 the environmental impacts of deep-sea mining activities (ISA 2010; Lodge et al., 2014;
 72 Madureira et al., 2016).

73 Although a considerable number of environmental impact studies have been conducted in
 74 different nodule fields, the prediction of environmental consequences of potential future deep-
 75 sea mining is still difficult (e.g., Ramirez-Llodra et al., 2011; Jones et al., 2017; Gollner et al.,
 76 2017; Cuvelier et al., 2018). In case of the CCZ, the evaluation of the environmental impact of
 77 deep-sea mining activities is challenging due to the fact that baseline data on the natural spatial
 78 heterogeneity and temporal variability of depositional conditions, benthic communities and the
 79 biogeochemical processes in the sediments are scarce (e.g., Mewes et al., 2014; 2016; Vanreusel
 80 et al., 2016; Mogollón et al., 2016; Juan et al., 2018; Volz et al., 2018; Menendez et al., 2018;
 81 Hauquier et al., under review). In addition, there is no clear consensus on the most appropriate
 82 mining techniques for the commercial exploitation of nodules, and technical challenges due to
 83 the inaccessibility of nodules at great water depths between 4000–5000 m have limited the
 84 deployment of deep-sea mining systems until today (e.g., Chung, 2010; Jones et al., 2017).

85 The physical removal of nodules as hard-substrate habitats has severe consequences for the
 86 nodule-associated sessile fauna as well as the mobile fauna (Bluhm, 2001; Smith et al., 2008;



87 Purser et al., 2016; Vanreusel et al., 2016). With slow nodule growth rates of a few
 88 millimeters per million years (e.g., Halbach et al., 1988; Kuhn et al., 2017a), the deep-sea fauna
 89 may not recover for millions of years (Vanreusel et al., 2016; Jones et al., 2017; Gollner et al.,
 90 2017; Stratmann et al., 2018). In addition to the removal of deep-sea fauna as well as seafloor
 91 habitats, the exploitation of nodules is associated with (1) the removal, mixing and re-
 92 suspension of the upper 4 cm to more than several tens of centimeters of the sediments, (2) the
 93 re-deposition of material from the suspended sediment plume, and (3) potentially also the
 94 compaction of the surface sediments due to weight of the nodule collector (Thiel, 2001; Oebius
 95 et al., 2001; König et al., 2001; Grupe et al., 2001; Radziejewska, 2002; Khripounoff et al.,
 96 2006; Cronan et al., 2010; Paul et al., 2018; Gillard et al., 2019). The wide range of estimations
 97 for the disturbance depth may be associated with (1) various devices used for the deep-sea
 98 disturbance experiments (Brockett and Richards, 1994; Oebius et al., 2001; Jones et al., 2017),
 99 (2) distinct sediment properties in different nodule fields of the Pacific Ocean (e.g., Cronan et
 100 al., 2010; Hauquier et al., under review) as well as (3) different approaches for the determination
 101 of the disturbance depth (e.g., Oebius et al., 2001; Grupe et al., 2001; Khripounoff et al., 2006).
 102 Based on the observation that bulk solid-phase Mn contents decrease over depth in the surface
 103 sediments of the DISCOL area, Paul et al. (2018) have suggested that the depth distribution of
 104 solid-phase Mn and associated metals (e.g., Mo, Ni, Co, Cu) could be used to trace the sediment
 105 removal by disturbances. In addition, other solid-phase properties such as organic carbon
 106 contents (TOC), porosity and radioisotopes may be suitable for the determination of the
 107 disturbance depth.

108 The most reactive TOC compounds, found in the bioturbated uppermost sediment layer, are the
 109 main drivers for early diagenetic processes (e.g., Froelich et al., 1979; Berner, 1981) and are
 110 expected to be removed during mining activities (König et al., 2001). Thus, strong
 111 biogeochemical implications can be expected in the sediments after deep-sea mining activities.
 112 König et al. (2001) have applied numerical modelling to study the consequences of the removal
 113 of the upper 10 cm of the sediments in the DISCOL area in the Peru Basin. They showed that
 114 the degradation of TOC during aerobic respiration, denitrification and Mn(IV) reduction may
 115 be decreased for centuries strongly influencing the oxygen penetration depth (OPD).

116 Here, we investigate the impact of various small-scale disturbances on geochemical conditions,
 117 biogeochemical processes and element fluxes in surface sediments of the CCZ. These small-
 118 scale disturbance tracks were created up to 37 years ago in four different European contract
 119 areas for the exploration of polymetallic nodules, including the German BGR (Bundesanstalt



120 für Geowissenschaften und Rohstoffe) area, the Belgian GSR (Global Sea Mineral Resources
 121 NV) area, the French IFREMER (Institut Français de Recherche pour l'Exploitation de la Mer)
 122 area and the Polish IOM (InterOceanMetal) area. In order to determine the disturbance depths
 123 of the different small-scale disturbances in the different European contract areas, we correlate
 124 the depth distributions of solid-phase Mn and total organic carbon (TOC) between disturbed
 125 sites and undisturbed reference sites using the Pearson product-moment correlation coefficient.
 126 On this basis, we (1) assess the short- and long-term consequences of small-scale disturbances
 127 on redox zonation and element fluxes and (2) determine how much time is needed for the re-
 128 establishment of a geochemical equilibrium in the sediments after the disturbances. Our work
 129 includes pore-water and solid-phase analyses as well as the application of a transient one-
 130 dimensional transport-reaction model.

131 2. Material and methods

132 As part of the European JPI Oceans pilot action “Ecological Aspects of Deep-Sea Mining
 133 (MiningImpact)”, multiple corer (MUC) and gravity corer (GC) sediment cores were taken
 134 during RV SONNE cruise SO239 in March/April 2015 from undisturbed sites in various
 135 European contract areas for the exploration of polymetallic nodules (Fig. 1; Table 1; Martínez
 136 Arbizu and Haeckel, 2015). These undisturbed reference sites were chosen in close proximity
 137 (< 5 km) to small-scale disturbance experiments for the simulation of deep-sea mining, which
 138 were created up to 37 yr ago and re-visited during cruise SO239 (Table 1; see Sect. 2.1.1.;
 139 Martínez Arbizu and Haeckel, 2015). The sampling of sediments in the disturbance tracks of
 140 these experiments were conducted by video-guided push-coring (PC) between 1 day and 37 yr
 141 after the initial disturbances using the ROV Kiel 6000 (Table 1; Fig. 2; Martínez Arbizu and
 142 Haeckel, 2015).

143 The different investigated European contract areas within the CCZ include the BGR, IOM, GSR
 144 and IFREMER areas. Comprehensive pore-water and solid-phase analyses on the MUC and
 145 GC sediment cores from undisturbed sites have been conducted in previous baseline studies
 146 and are presented elsewhere (Volz et al., 2018; Volz et al., under review). These analyses
 147 include the determination of pore-water oxygen, NO_3^- , Mn^{2+} and NH_4^+ concentrations and
 148 contents of total organic carbon (TOC) for MUC and GC sediment cores (Volz et al., 2018) as
 149 well as solid-phase bulk Mn contents for the MUC sediment cores (Volz et al., under review).
 150 In the framework of this study, we have used these previously published pore-water and solid-
 151 phase data as undisturbed reference data for geochemical conditions and sediment composition



(Table 1). On this basis, here, we investigate seven small-scale disturbances for the simulation of deep-sea mining (Table 1; see Sect. 2.1.1.; Martínez Arbizu and Haeckel, 2015).

2.1. Site Description

The CCZ is defined by two transform faults, the Clarion Fracture Zone in the north and the Clipperton Fracture Zone in the south and covers an area of about 6 million km² (Fig. 1; e.g., Halbach et al., 1988). The sediments at the investigated sites (Table 1) are dominated by clayey siliceous oozes with various Mn nodule sizes (1–10 cm) and spatial densities (0–30 kg m⁻²) at the sediment surface (Berger, 1974; Kuhn et al., 2012; Mewes et al., 2014; Volz et al., 2018). In order to characterize the investigated sediments with respect to redox zonation, sedimentation rates, fluxes of particulate organic carbon (POC) to the seafloor and bioturbation depths, we have summarized these key parameters, which are originally presented elsewhere, in Table 2 (Volz et al., 2018). Steady state transport-reaction models have shown that aerobic respiration is the dominant biogeochemical process at all investigated sites, consuming more than 90 % of the organic matter delivered to the seafloor (Mogollón et al., 2016; Volz et al., 2018). Below the OPD at more than 0.5 m depth, Mn(IV) and nitrate reduction succeeds in the suboxic zone, where oxygen and sulfide are absent (e.g., Mewes et al., 2014; Mogollón et al., 2016; Kuhn et al., 2017b; Volz et al., 2018). At several sites investigated in this study, including the BGR “reference area” (BGR-RA) and IOM sites, decreasing Mn²⁺ concentrations at depth are probably associated with the oxidation of Mn²⁺ by upward diffusing oxygen circulating through the underlying basaltic crust (Volz et al., 2018; Mewes et al., 2016; Kuhn et al., 2017b).

2.1.1. Small-scale disturbances

Since the 1970s, several comprehensive environmental impact studies of deep-sea mining simulations have been carried out in the CCZ, including the Benthic Impact Experiment (BIE; e.g., Trueblood and Ozturgut, 1997; Radziejewska, 2002) and the Japan Deep Sea Impact Experiment (JET; Fukushima, 1995). In addition, numerous small-scale seafloor disturbances have been carried out in the CCZ in the past 40 yr using various tools such as epibenthic sleds (EBS) and dredges (e.g., Vanreusel et al., 2016; Jones et al., 2017). The EBS is towed along the seabed for the collection of benthic organisms (and nodules) thereby also removing the upper few centimeters of the sediments (e.g., Brenke, 2005). In 2015, some of these disturbances were re-visited as part of the BMBF-EU JPI Oceans pilot action “Ecological Aspects of Deep-Sea Mining (MiningImpact)” project in order to evaluate the long-term consequences of such small-scale disturbances on the abyssal benthic ecosystem (Martínez Arbizu and Haeckel, 2015). For comparison, the Disturbance and Recolonization Experiment (DISCOL), which was conducted



185 in a nodule field in the Peru Basin (PB) in 1989 was re-visited as part of MiningImpact (Boetius,
 186 2015; Greinert, 2015). In the framework of DISCOL, a seafloor area of $\sim 11 \text{ km}^2$ was disturbed
 187 with a plough harrow. The impact of the DISCOL experiment was studied 0.5, 3 and 7 yr after
 188 the disturbance had been set (e.g., Thiel, 2001).

189 Comparably small-scale, up to 37 yr old simulations of deep-sea mining in various European
 190 contract areas within the CCZ were re-visited in 2015 during the RV SONNE cruise SO239
 191 (Table 1; Fig. 2; Martínez Arbizu and Haeckel, 2015). New small-scale disturbance tracks were
 192 created during SO239 in the BGR-RA and in the GSR area “B6” using an EBS in order to add
 193 also initial temporal datasets (Table 1; Fig. 2; Martínez Arbizu and Haeckel, 2015). The EBS
 194 weighed about 400 kg under normal atmospheric pressure and created a disturbance track of
 195 about 1.5 m width (Brenke, 2005). The fresh EBS disturbance tracks in the BGR-RA and GSR
 196 areas were re-visited 1 day after their creation. Eight months prior to the cruise SO239, towed
 197 dredge sampling was performed in the GSR area by the Belgian contractor (Martínez Arbizu
 198 and Haeckel, 2015; Jones et al., 2017). During the BIONOD cruises onboard RV L’Atalante in
 199 2012, the same EBS setup as used during cruise SO239 was deployed in the BGR “prospective
 200 area” (BGR-PA) and in the IFREMER area (Table 1; Rühlemann and Menot, 2012; Menot and
 201 Rühlemann, 2013; Martínez Arbizu and Haeckel, 2015). In 1995, the Deep-Sea Sediment Re-
 202 suspension System (DSSRS) was used during the IOM-BIE (Benthic Impact Experiment)
 203 disturbance in the IOM area (Table 1; e.g., Kotlinski and Stoyanova, 1998). The DSSRS
 204 weighed 3.2 tons under normal atmospheric pressure and was designed to dredge the seafloor
 205 while producing a re-suspended particle plume about 5 m above the seafloor (Brockett and
 206 Richards, 1994; Sharma, 2001). Based on the dimensions of the DSSRS device, the disturbance
 207 track created during the IOM-BIE disturbance experiment is about 2.5 m wide (Fig. 2; Brockett
 208 and Richards, 1994). In 1978, the Ocean Mineral Company (OMCO) created disturbance tracks
 209 in the French IFREMER area by towed dredge sampling (Table 1; e.g., Spickermann, 2012).

210 **2.2. Sediment sampling and solid-phase analyses**

211 ROV-operated push cores were sampled at intervals of 1 cm for solid-phase analyses. Bulk
 212 sediment data and TOC contents have been corrected after Kuhn (2013) for the interference of
 213 the pore-water salt matrix with the sediment composition (Volz et al., 2018). The salt-free
 214 volume fraction of the pore water, i.e. the porosity, was determined gravimetrically before and
 215 after freeze drying of the wet sediment samples. The salt-corrected sediment composition c'
 216 was calculated from the measured solid-phase composition c using the mass percentage of H_2O
 217 of the wet sediment (w), which contains 96.5 % H_2O (Eq. (1)).



$$c' = c * \frac{100}{100 - (100 * \frac{100}{(w * \frac{100}{96.5}) - w})} \quad (1)$$

2.2.1. Total acid digestions

Total acid digestions were performed in the microwave system MARS Xpress (CEM) after the protocols by Kretschmer et al. (2010) and Nöthen and Kasten (2011). Approximately 50 mg of freeze-dried, homogenized bulk sediment were digested in an acid mixture of 65 % sub-boiling distilled HNO_3 (3 mL), 30 % sub-boiling distilled HCl (2 mL) and 40 % suprapur® HF (0.5 mL) at $\sim 230^\circ\text{C}$. Digested solutions were fumed off to dryness, the residue was re-dissolved under pressure in 1 M HNO_3 (5 mL) at $\sim 200^\circ\text{C}$ and then filled up to 50 mL with 1 M HNO_3 . Total bulk Mn and Al contents were determined using inductively coupled plasma optical emission spectrometry (ICP-OES; IRIS Intrepid ICP-OES Spectrometer, Thermo Elemental). Based on the standard reference material NIST 2702 accuracy and precision of the analysis was 3.7 % and 3.5 % for Mn, respectively ($n=67$).

2.2.2. Total organic carbon

Total organic carbon (TOC) contents were determined using an Eltra CS2000 element analyzer. Approximately 100 mg of freeze-dried, homogenized sediment were transferred into a ceramic cup and decalcified with 0.5 mL of 10 % HCl at 250°C for 2 h before analysis. Based on an in-house reference material, precision of the analysis was better than 3.7 % ($n=83$).

2.3. Pearson correlation coefficient

In order to determine the disturbance depths, solid-phase bulk Mn contents were correlated between disturbed sediments and undisturbed reference sediments using the Pearson product-moment correlation coefficient r (Eq. (2); Table 1; Pearson, 1895). The Pearson correlation coefficient is a statistical measure of the linear relationship between two arrays of variables with:

$$r = \frac{\sum_{i=1}^n (x - \bar{x})(y - \bar{y})}{\sqrt{\sum_{i=1}^n (x - \bar{x})^2 \sum_{i=1}^n (y - \bar{y})^2}} \quad (2)$$

where n is the sample size, x and y are individual sample points and \bar{x} and \bar{y} are the sample means $\bar{x} = \frac{1}{n} \sum_{i=1}^n x$ and $\bar{y} = \frac{1}{n} \sum_{i=1}^n y$.

While the solid-phase bulk Mn contents of the disturbed sediments were determined in the framework of this study, solid-phase bulk Mn contents from undisturbed reference sediments were taken from Volz et al. (under review). The highest positive linear correlations of solid-



phase Mn contents ($r_{\text{Mn}} \sim 1$) between the disturbed sites and the respective undisturbed reference sites (Table 1) were used to determine the depths of the disturbances. In a second step, the same correlation was applied to the TOC contents (r_{TOC}) in order to verify the depth of disturbance. While the TOC contents in the disturbed sediments were determined in the framework of this study, TOC contents from undisturbed reference sediments were taken from Volz et al. (2018).

2.4. Geochemical model setup and reaction network

A transient one-dimensional transport-reaction model (Eq. (3); e.g., Boudreau, 1997; Haeckel et al., 2001; Boudreau, 1997) was used (1) to assess the impact of small-scale disturbances on biogeochemical processes, geochemical conditions and element fluxes in sediments of the CCZ and (2) to estimate the time required to establish a new geochemical equilibrium after a small-scale disturbance. We have applied the transient transport-reaction model for the sites in the BGR-RA and IOM areas (Table 1). These sites were chosen due to distinctively different sedimentation rates and OPD (Table 2). We have adapted the steady state transport-reaction model, which was originally presented by Volz et al. (2018) and used pore-water oxygen, NO_3^- , Mn^{2+} and NH_4^+ data as well as TOC contents of GC sediment cores from the same study as undisturbed reference data (Table 1; Table 2). The transient transport-reaction model consists of four aqueous (O_2 , NO_3^- , Mn^{2+} , NH_4^+), four solid species (TOC_{1-3} , MnO_2) and six reactions ($\text{R}_1\text{-R}_6$; Supplementary Table 1) with:

$$\frac{\partial(\vartheta_i C_{i,j})}{\partial t} = \frac{\partial D_{i,j} \vartheta_i \left(\frac{\partial C_{i,j}}{\partial z} \right)}{\partial z} - \frac{\partial \omega_i \vartheta_i C_{i,j}}{\partial z} + \alpha_i \vartheta_i (C_{i,j} - C_{0,j}) + \vartheta_i \sum R_{i,j} \quad (3)$$

where z is sediment depth, and subscripts i, j represent depth and species-dependence, respectively; aqueous or solid species concentration are denoted by C (Supplementary Table 2); D is in case of solutes the effective diffusive mixing coefficient, which has been corrected for tortuosity ($D_{m,i,j}$; Boudreau, 1997). In the case of solids, D represents the bioturbation coefficient (B_i ; Eq. (4)); ϑ is the volume fraction representing the porosity φ for the aqueous phase and $1 - \varphi$ for the solid phase; the velocity of either the aqueous (v) or the solid phase (w) is denoted by the symbol ω ; α_i is the bioirrigation coefficient (0 for solid species; Eq. (5)); and $\sum R_{i,j}$ is the sum of the reactions affecting the given species.

The bioturbation and bioirrigation profiles, i.e. biologically induced mixing of sediment and pore water, respectively, are represented by a modified logistic function:

$$B_i = B_0 \exp\left(\frac{z_{\text{mix}} - z_i}{z_{\text{att}}}\right) / \left(1 + \exp\left(\frac{z_{\text{mix}} - z_i}{z_{\text{att}}}\right)\right) \quad (4)$$



$$\alpha_i = \alpha_0 \exp\left(\frac{z_{mix} - z_i}{z_{att}}\right) / \left(1 + \exp\left(\frac{z_{mix} - z_i}{z_{att}}\right)\right) \quad (5)$$

where α_0 and B_0 are constants indicating the maximum biorrigation and bioturbation intensity at the sediment-water interface; the depth where the bioturbation and bioirrigation intensity is halved is denoted by z_{mix} ; and the attenuation of the biogenically induced mixing with depth is controlled by z_{att} .

Assuming steady-state compaction, the model applies an exponential function that is parameterized according to the available porosity data at each station (e.g., Berner, 1980; Supplementary Fig. 1):

$$\varphi_i = \varphi_\infty (\varphi_0 - \varphi_\infty) \exp(-\beta z) \quad (6)$$

where φ_∞ is the porosity at the ‘infinite depth’, at which point compaction is completed; φ_0 is the porosity at the sediment water interface ($z = 0$); and β is the porosity-attenuation coefficient.

Organic matter was treated in three reactive fractions (3G-model) with first order kinetics. The rate expressions for the reactions (R_1 - R_6) include inhibition terms, which are listed together with the rate constants (Supplementary Table 3).

Based on the Pearson correlation coefficient r_{Mn} , we have removed the upper 7 cm of sediments in the transport-reaction model for the IOM-BIE site and the upper 10 cm of sediments in the transport-reaction model for the BGR-RA site. Due to the lack of data on the re-establishment of bioturbation, i.e. the recovery of the bioturbation ‘pump’ after small-scale disturbance experiments, we have tested the effect of different bioturbation scenarios in the transport-reaction model. For the different post-disturbance bioturbation scenarios, we have assumed that bioturbation is inhibited immediately after the disturbance with a linear increase to undisturbed reference bioturbation coefficients (Volz et al., 2018). Based on the work by Miljutin et al. (2011) and Vanreusel et al. (2016), we have assumed that bioturbation should be fully re-established after 100, 200, and 500 yr. As the modelling results for the different time spans were almost identical, we only present here the model that assumes bioturbation is at pre-disturbance intensity 100 yr after the impact (Volz et al., 2018; Supplementary Table 2). We have applied the transient transport-reaction model under the assumption that the sedimentation rates as well as the POC fluxes to the seafloor remain constant over time (Table 2). The model was coded in MATLAB with a discretization and reaction set-up closely following the steady state model (Volz et al., 2018).



3. Results

3.1. Characterization of disturbed sites

Most of the small-scale disturbances investigated in the framework of this study were created with an EBS (Table 1; Fig. 2). Based on the visual impact inspection of the EBS disturbance tracks in the CCZ, the sediments were mostly pushed aside by the EBS and piled up next to the left and right of the tracks (Fig. 2). In particular, the freshly created 1-day old EBS tracks in the BGR-RA and GSR areas indicate that the sediments were mostly scraped off and accumulated next to the freshly exposed sediment surfaces (Fig. 2). Small sediment lumps occur on top of the exposed sediment surfaces on the EBS tracks, which indicates that some sediment has slid off from the adjacent flanks of the sediment accumulation after the disturbances (Fig. 2). However, the mostly smooth sediment surfaces of the EBS tracks suggest that sediment mixing during the EBS disturbance experiments may be mostly negligible (Fig. 2; Table 1). In the 8-months old dredge track in the GSR area, small furrows occur at the disturbed sediment surface most likely caused by the shape of the dredge (Fig. 2).

3.2. Sediment porosity and solid-phase composition

The sediment porosity shows little lateral variability and ranges between 0.65 and 0.8 throughout the upper 25 cm of the sediments at all investigated disturbed sites (Fig. 3). At the disturbed IOM-BIE site, sediment porosity is about 5 % higher in the upper 4 cm of the sediments than below. Total bulk Mn contents in the upper 25 cm of the sediments at the disturbed sites are between 0.1 and 0.9 wt% (Fig. 3). Solid-phase Mn contents decrease with depth at all investigated sites. Total organic carbon (TOC) contents in the upper 25 cm of the sediments at the disturbed sites are within 0.2 and 0.5 wt% (Fig. 3). The TOC contents slightly decrease with depth at all investigated sites.

3.3. Pearson correlation coefficient and disturbance depths

The Pearson correlation coefficient r_{Mn} for the correlation of solid-phase Mn contents between the disturbed sites and the respective reference sites ranges between 0.72 and 0.97 (Table 3). Based on r_{Mn} , 5-15 cm of sediment has been removed by various disturbance experiments in the different contract areas (Fig. 4). Applying these r_{Mn} -derived disturbance depths for the correlation of the TOC depth distributions between disturbed sites and respective adjacent reference sites gives Pearson correlation coefficients r_{TOC} within 0.73 and 0.91 (Table 3; Fig. 4), which may support the estimates for the disturbance depth based on r_{Mn} . At the BGR-RA site, the correlation of TOC contents between the disturbed site and the reference site shows negative values. As the sediment porosity in the disturbed sediments correlates well with the



porosity in the respective undisturbed reference sediments (Fig. 4), sediment compaction due to the weight of the disturbance device may be negligible during the small-scale disturbances investigated in the framework of this study.

3.4. Transport-reaction modelling

The removal of the surface sediments in the transient transport-reaction model for the BGR-RA and IOM-BIE sites is associated with the loss of the reactive labile organic matter (Fig. 5 and 6). About 10 kyr after the removal of the upper 10 cm of the sediments in the model for the BGR-RA site, oxygen penetrates about tenfold deeper into the disturbed sediments than in undisturbed sediments (Table 2; Fig. 5; Volz et al., 2018). At the IOM-BIE site, oxygen reaches the maximum OPD at about 100 yr after the removal of the upper 7 cm of the sediments. At this site, the oxygen front migrates only ~1 m deeper than the corresponding OPD in undisturbed sediments (Table 2; Fig. 5; Volz et al., 2018). As a consequence of deeper OPDs at both sites, the oxic-suboxic redox boundary is located at greater depth, with a significant consumption of pore-water Mn^{2+} in the path of the oxygen front. The NH_4^+ concentrations are also being diminished, reaching minima within 100-1000 yr and 1-10 yr after the disturbance experiments in the BGR-RA and IOM areas, respectively. The trend for the NO_3^- is more complicated with lower concentrations during the downward migration of the OPD and augmented concentrations once oxygen concentrations reach their maximum (Figs. 5 and 6).

Naturally, the solute fluxes across the sediment-water interface (SWI) are strongly affected after the surface sediment removal (Fig. 7). The transient transport-reaction model suggests that the oxygen fluxes into the sediments are lowered by a factor of three to six after 10-100 yr at the IOM-BIE and BGR-RA sites, respectively. This trend is mirrored by the decreased release of NH_4^+ and NO_3^- into the bottom water.

4. Discussion

4.1. Depths of small-scale disturbance experiments

Our work demonstrates that the depth distribution of solid-phase Mn provides a reliable tool for the determination of the disturbance depths in the sediments of the CCZ (Fig. 4; Table 3). The success of the correlation of solid-phase Mn contents between disturbed and undisturbed reference sediments benefits from several factors:

(1) Sediment mixing during the small-scale disturbance experiments is negligible: The visual impact assessment of the investigated disturbance tracks in the CCZ suggests that sediment mixing during the small-scale disturbance experiments was insignificant (Fig. 2). This



374 observation is in agreement with a recent EBS disturbance experiment, which has been
375 conducted in the DISCOL area in 2015 (Greinert, 2015). The freshly created EBS track in the
376 DISCOL area was re-visited 5 weeks after the disturbance experiment, where the surface
377 sediment was mostly removed and deeper sediment layers were exposed without visible
378 sediment mixing (Boetius, 2015; Paul et al., 2018). In a study on the geochemical regeneration
379 in disturbed sediments of the DISCOL area in the Peru Basin, Paul et al. (2018) have shown
380 that the bulk Mn-rich top sediment layer, which has been observed in undisturbed sediments, is
381 removed in the 5-week old EBS disturbance track. Thus, an important pre-requisite for this
382 method is met and the authors have proposed that the depth distribution of solid-phase Mn may
383 be suitable for the evaluation of the impact as well as for the monitoring of the recovery of
384 small-scale disturbance experiments.

385 (2) The fact that the solid-phase Mn maxima in the surface sediments of the CCZ appear to be
386 a regional phenomenon (Volz et al., under review): The investigated disturbed sediments as
387 well as the undisturbed reference sediments in the CCZ show decreasing solid-phase Mn
388 contents with depth in the upper 20-30 cm of the sediments (Fig. 3; Fig. 4; Volz et al., under
389 review). In the undisturbed reference sediments, solid-phase Mn contents show maxima of up
390 to 1 wt% in the upper 10 cm of the sediments with distinctly decreasing contents below (Fig. 4;
391 Volz et al., under review). Similar bulk solid-phase Mn distribution patterns have been reported
392 for other sites within the CCZ (e.g., Khripounoff et al., 2006; Mewes et al., 2014; Widmann et
393 al., 2014). Volz et al. (under review) have suggested that the widely observed solid-phase Mn
394 enrichments in the surface sediments of the CCZ formed in association with a more compressed
395 redox zonation, which may have prevailed during the last glacial period as a result of lower
396 bottom-water oxygen concentrations than today. As a consequence of this condensed redox
397 zonation, upward diffusing pore-water Mn^{2+} may have precipitated as authigenic Mn(IV) at a
398 shallow oxic-suboxic redox boundary in the upper few centimeters of the sediments. After the
399 last glacial period, the authigenic Mn(IV) peak was continuously mixed into subsequently
400 deposited sediments by bioturbation causing the observed broad solid-phase Mn(IV)
401 enrichment in the surface sediments (Fig. 4; Volz et al., under review).

402 (3) Lastly, the OPD at all sites is located at sediment depths greater than 0.5 m, and thus,
403 diagenetic precipitation of Mn(IV) in the surface sediments (e.g. Gingele and Kasten, 1994)
404 since the last glacial period can be ruled out (Table 2; Mewes et al., 2014; Volz et al., under
405 review).



406 Based on the depth distribution of solid-phase Mn, our work suggests that between 5 and 15 cm
407 of the surface sediments were removed by the different small-scale disturbance experiments in
408 the CCZ (Table 3; Fig. 4). This range of disturbance depths is in good agreement with other
409 estimates for small-scale disturbances by similar gear in the CCZ and in the DISCOL area,
410 which suggest that the upper 4-20 cm of the sediments were removed (e.g., Thiel, 2001; Oebius
411 et al., 2001; König et al., 2001; Grupe et al., 2001; Radziejewska, 2002; Khripounoff et al.,
412 2006; Paul et al., 2018). However, as the disturbed sites investigated in this study and the
413 respective undisturbed reference sites are located up to 5 km apart from each other, the
414 correlation of solid-phase Mn may be influenced by some spatial heterogeneities in solid-phase
415 Mn contents (Table 1; Mewes et al., 2014). Furthermore, it should be noted, that for the
416 correlation of solid-phase Mn contents between the disturbed and undisturbed reference sites,
417 we have not considered that (1) particles may have re-settled on the freshly exposed sediment
418 surfaces from re-suspended particle plumes (e.g., Jankowski and Zielke, 2001; Thiel, 2001;
419 Radziejewska, 2002; Gillard et al., 2019), (2) sediment has slid off from adjacent flanks of the
420 sediment accumulation after the disturbances (Fig. 2) and (3) sediments have been deposited
421 after the small-scale disturbances at sedimentation rates between 0.2 and 1.2 cm kyr⁻¹ (Table 2;
422 Volz et al., 2018). However, only in the case of the IOM-BIE disturbance, the visual impact
423 assessment suggested that the disturbance surface was concealed, here by re-settling sediments
424 (Fig. 2). The development of a re-suspended particle plume during the disturbance experiments
425 highly depends on various factors, such as sediment properties, seafloor topography, bottom-
426 water currents and the disturbance device (e.g., Gillard et al., 2019). Although local and regional
427 variations in these factors have been reported for the CCZ, they are not well constrained (e.g.,
428 Mewes et al., 2014; Aleynik et al., 2017; Volz et al., 2018; Gillard et al., 2019; Hauquier et al.,
429 under review). As the disturbance tracks investigated in the framework of this study are
430 relatively small with a maximum width of 2.5 m (Fig. 2; Brockett and Richards, 1994; Brenke
431 2005), re-suspended particles may (1) only partly deposit on the disturbance track and (2)
432 mostly be transported laterally by currents and deposit on top of undisturbed sediments in the
433 proximity of the disturbance tracks (e.g., Fukushima, 1995; Aleynik et al., 2017; Gillard et al.,
434 2019). This is in accordance with the close correlation of the sediment porosity between the
435 disturbed and undisturbed reference sites, which indicates that the deposition of re-settling
436 particles with higher porosity at the sediment surface in the disturbance tracks is insignificant
437 at all sites, except for the IOM-BIE site (Fig. 4). The porosity data further shows that sediment
438 compaction, potentially caused by the weight of the disturbance device (Cuvelier et al., 2018;
439 Hauquier et al., under review) is insignificant at all disturbed sites.



4.2. Impact of small-scale disturbances on the geochemical system

The geochemical conditions found at the study sites in the CCZ are the result of a balanced interplay of key factors, such as the input of fresh, labile TOC, sedimentation rate and bioturbation intensity (e.g., Froelich et al., 1979; Berner, 1981; Zonneveld et al., 2010; Mogollón et al., 2016; Volz et al., 2018). Together they characterize the upper reactive layer, which in turn plays a crucial role for the location of the OPD in the sediments of the CCZ (e.g., Mewes et al., 2014; Mogollón et al., 2016; Volz et al., 2018). Oxygen is consumed via aerobic respiration during the degradation of organic matter while bioturbation transports fresh, labile TOC into deeper sediments (e.g., Haeckel et al., 2001; König et al., 2001). The presence of labile TOC throughout the bioturbated zone significantly enhances the consumption of oxygen with depth, where oxygen is not as easily replenished by seawater oxygen. Thus, the availability of labile TOC in the bioturbated layer controls the amount of oxygen that passes through the reactive layer into deeper sediments (e.g., König et al., 2001). Below the highly reactive layer, refractory organic matter degradation and secondary redox reactions – such as oxidation of Mn^{2+} – control the consumption of oxygen (Supplementary Table 1; Mogollón et al., 2016; Volz et al., 2018). The oxygen profile, more precisely the position of the OPD, in turn, strongly influences the distribution of other solutes. Below the OPD, denitrification and Mn(IV) reduction commence, albeit at much lower rates, consuming pore-water NO_3^- and releasing Mn^{2+} (Mogollón et al., 2016; Volz et al., 2018). The study sites in the CCZ provide an excellent example for how slight differences in key environmental factors can profoundly change the overall solute profiles with OPDs ranging between 0.5 m (BGR-RA) and > 7.4 m (GSR) as outlined by Volz et al. (2018).

Mining-related removal of the upper 5–15 cm of the sediment results, on one hand, in an almost complete loss of the labile TOC fraction (Fig. 4) as this fraction is restricted to the upper 20 cm of the sediment in the CCZ (e.g., Müller and Mangini, 1980; Emerson, 1985; Müller et al., 1988; Mewes et al., 2014; Mogollón et al., 2016; Volz et al., 2018). On the other hand, studies on faunal diversity and density in small-scale disturbances in the sediments of the CCZ and in the DISCOL area show that most of the biota is lost immediately after the disturbance experiment (Borowski et al., 1998; 2001; Bluhm et al., 2001; Thiel et al., 2001; Vanreusel et al., 2016; Jones et al., 2017; Gollner et al., 2017). Thus, a drastic decline or stand-still of bioturbation can be expected in the surface sediments.

Based on the results of the transient transport-reaction model, geochemical recovery after small-scale sediment disturbances can be divided into two main phases (Fig. 8):



473 (1) Since the labile TOC fraction and bioturbating fauna is mostly removed, downward
 474 diffusion of oxygen is the main driver shaping solute profiles towards a new geochemical
 475 equilibrium in the absence of the reactive layer (Figs. 5 and 6). This entails the downward
 476 migration of the OPD, as oxygen is no longer effectively consumed in the upper sediment layer.
 477 The presence of oxygen outcompetes denitrification and Mn(IV) reduction and induces NH_4^+
 478 and Mn^{2+} oxidation instead, thus, minimizing pore-water NH_4^+ and Mn^{2+} concentrations
 479 (Figs. 5 and 6). At the same time, NO_3^- , as a by-product of aerobic-respiration (e.g., Froelich et
 480 al., 1979; Berner, 1981; Haeckel et al., 2001; Mogollón et al., 2016; Volz et al., 2018), is
 481 accordingly reduced during denitrification and NO_3^- concentrations are lowered during this first
 482 phase.

483 (2) The second phase is characterized by the increasing influence of reactive fluxes across the
 484 seafloor. It takes approximately 1000 yr before any significant build-up of an upper labile TOC
 485 layer is re-established (Fig. 6), at which point solute profiles slowly shift towards their pre-
 486 disturbance shape (Fig. 7). Interestingly, during the transition time when oxygen is still present
 487 at depth but aerobic respiration in the upper sediments has already begun to pick up, NO_3^-
 488 concentrations are strongly elevated in the BGR sediments (Figs. 5 and 6). This is due to the
 489 fact that NO_3^- is not consumed during denitrification or the Mn-annamox reaction in the
 490 presence of oxygen (Mogollón et al., 2016; Volz et al., 2018).

491 With the importance of bioturbation and the mining-related removal of associated fauna in
 492 mind, solute and in particular nutrient fluxes across the seafloor should also be considered. The
 493 release of nutrients complements the close link between sediment geochemistry and the food
 494 web structure (e.g., Smith et al., 1979; Dunlop et al., 2016; Stratmann et al., 2018) and further
 495 emphasizes their interdependencies. Figure 7 depicts fluxes of oxygen, NO_3^- and NH_4^+ across
 496 the seafloor. As expected, with the reactive layer being mostly absent, fluxes across the seafloor
 497 are severely reduced, which particularly affects the oxygen uptake of the sediments as well as
 498 the release of NO_3^- and NH_4^+ into the bottom water. At about 100 to 1000 yr after the
 499 disturbance, concurrent with the build-up of an upper sediment layer containing significant
 500 amounts of labile organic matter, fluxes begin to increase again, albeit much slower than the
 501 rate of the decrease in fluxes subsequently after the disturbances (Fig. 7, note the logarithmic
 502 scale).

503 It should be noted that while bioturbation has a pivotal influence on the undisturbed steady-
 504 state profile, it only plays a secondary role in re-establishing the geochemical equilibrium at the
 505 disturbed sites in the CCZ. Studies suggest that faunal abundances fully recover within centuries



506 after the disturbance even though the benthic community may be different than prior to the
507 disturbance (e.g., Miljutin et al., 2011; Vanreusel et al., 2016). Due to the extremely slow build-
508 up of the reactive layer with labile TOC, the bioturbation ‘pump’ is active again before any
509 significant amount of labile TOC is present about 1-100 kyr after the disturbance. Thus, full
510 recovery is mainly controlled by the re-establishment of the upper reactive layer, i.e. the
511 accumulation rate of labile TOC on the seafloor.

512 The transport-reaction model reveals that under current depositional conditions, the re-
513 equilibrated geochemical system is established after 1-10 kyr at the IOM-BIE site, while the re-
514 establishment of the geochemical equilibrium at the BGR-RA site takes 10-100 kyr
515 (Figs. 5 and 6). Shorter recovery times at the IOM site compared to the BGR-RA site are related
516 to higher sedimentation rates (1.15 instead of 0.65 cm kyr⁻¹) and shallower impact on the
517 sediment (7 cm instead of 10 cm sediment removal). Accordingly, the maximum OPD is
518 reached after 100 yr and 10 kyr at the IOM and BGR-RA site, respectively (Figs. 5 and 6) while
519 the reactive layer is clearly established sooner at the IOM site compared to the BGR-RA site
520 (Fig. 7). Thus, the disturbance depth clearly has a strong influence on the recovery process of
521 the geochemical system of the sediments, highlighting the importance of low-impact mining
522 equipment. Considering that in the CCZ areas of about 8500 km² could be commercially mined
523 in 20 yr per individual mining operation (Madureira et al., 2016), this impact assessment of
524 small-scale disturbance experiments may only represent a first approach for the prediction of
525 the environmental impact of large-scale deep-sea mining activities.

526 5. Conclusion

527 We have studied surface sediments from seven small-scale disturbance experiments for the
528 simulation of deep-sea mining, which were performed between 1 day and 37 years prior to our
529 sampling in the NE Pacific Ocean. These small-scale disturbance tracks were created using
530 various disturbance devices in different European contract areas for the exploration of
531 polymetallic nodules within the eastern part of the Clarion-Clipperton Zone (CCZ). Through
532 correlation of solid-phase Mn contents of disturbed and undisturbed reference sediments, we
533 (1) propose that the depth distribution of solid-phase Mn in the sediments of the CCZ provides
534 a reliable tool for the estimation of the disturbance depth and (2) show that 5-15 cm of the
535 sediments were removed during the small-scale disturbance experiments investigated in this
536 study. As the small-scale disturbances are associated with the removal of the surface sediments
537 characterized by reactive labile organic matter, the disturbance depth ultimately determines the
538 impact on the geochemical system in the sediments. The application of a transient transport-



539 reaction model reveals that the removal of the upper 7-10 cm of the surface sediments is
540 associated with a meter-scale downward extension of the oxic zone and the shutdown of
541 denitrification and Mn(IV) reduction. As a consequence of lower respiration rates after the
542 disturbance experiments, the geochemical system in the sediments is controlled by downward
543 oxygen diffusion. While the re-establishment of bioturbation within centuries after the
544 disturbance is important for the geochemical re-equilibration in the disturbed sediments, the
545 rate at which the new geochemical system re-equilibrates ultimately depends on the burial rate
546 of organic matter. Assuming the accumulation of labile organic matter to proceed at current
547 Holocene sedimentation rates in the disturbed sediments, biogeochemical reactions resume in
548 the reactive surface sediment layer, and thus, the new geochemical equilibrium in the disturbed
549 sediments in the CCZ is reached on a millennial time scale after the disturbance of the surface
550 sediments.

551 Our study represents the first study on the impact of small-scale disturbance experiments on the
552 sedimentary geochemical system in the prospective areas for polymetallic nodule mining in the
553 CCZ. Our findings on the evaluation of the disturbance depths using solid-phase Mn contents
554 as well as the quantification of the geochemical re-equilibration in the sediments advances our
555 knowledge about the potential long-term consequences of deep-sea mining activities. We
556 propose that mining techniques potentially used for the potential commercial exploitation of
557 nodules in the CCZ may remove less than 10 cm of the surface sediments in order to minimize
558 the impact on the geochemical system in the sediments. Furthermore, the depth distribution of
559 solid-phase Mn may be used for environmental monitoring purposes during future mining
560 activities in the CCZ. This study also provides valuable data for further investigations on the
561 environmental impact of deep-sea mining, such as during the launched JPI Oceans follow-up
562 project MiningImpact 2.

563 **Data availability**

564 The data are available via the data management portal OSIS-Kiel and the WDC database
565 PANGAEA, including the solid-phase bulk sediment Mn and TOC contents
566 (<https://doi.org/10.1594/PANGAEA.904560>) as well as the porosity data
567 (<https://doi.org/10.1594/PANGAEA.904578>).

568 **Author contribution**

569 The study was conceived by all co-authors. JBV carried out the sampling and analyses on board
570 during RV SONNE cruise SO239 and the analytical work in the laboratories at AWI in



571 Bremerhaven. LH and MH modified the numerical transport-reaction model presented in Volz
572 et al. (2018) and provided model results for the long-term effects of small-scale disturbances
573 on geochemical conditions and biogeochemical processes. JBV prepared the manuscript with
574 substantial contributions from all co-authors.

575 **Competing interest**

576 The authors declare that they have no conflict of interest.

577 **Acknowledgements**

578 We thank captain Lutz Mallon, the crew and the scientific party of RV SONNE cruise SO239
579 for the technical and scientific support. Thanks to Jennifer Ciomber, Benjamin Löffler and
580 Vincent Ozegowski for their participation in sampling and analysis onboard. For analytical
581 support in the home laboratory and during data evaluation we are grateful to Ingrid Stimac, Olaf
582 Kreft, Dennis Köhler, Ingrid Dohrmann (all at AWI). Special thanks to Prof. Dr. Gerhard
583 Bohrmann (MARUM, University of Bremen), Dr. Timothy G. Ferdelman (MPI Bremen) and
584 Dr. Ellen Pape (University of Ghent) for much appreciated discussions.

585 This study is funded by the Bundesministerium für Bildung und Forschung (BMBF Grant
586 03F0707A+G) as part of the JPI-Oceans pilot action “Ecological Aspects of Deep-Sea Mining
587 (MiningImpact)”. We acknowledge further financial support from the Helmholtz Association
588 (Alfred Wegener Institute Helmholtz Centre for Polar and Marine Research).



589 References

- 590 Aleynik, D., Inall, M. E., Dale, A., and Vink, A.: Impact of remotely generated eddies on plume
 591 dispersion at abyssal mining sites in the Pacific, *Sci. Rep.*, 7, 1–14, doi:10.1038/s41598-
 592 017-16912-2, 2017.
- 593 Berger, W. H.: Deep-sea sedimentation, in: *The Geology of Continental Margins*, edited by:
 594 Burk, C. A., and Drake, C. L., Springer, New York, 213–241, 1974.
- 595 Berner, R. A.: A new geochemical classification of sedimentary environments, *J. Sediment.*
 596 *Petrol.*, 51, 359–365, 1981.
- 597 Berner, R. A.: *Early Diagenesis: A Theoretical Approach*, Princeton University Press,
 598 Princeton, 1–24, 1980.
- 599 Bluhm H.: Re-establishment of an abyssal megabenthic community after experimental physical
 600 disturbance of the seafloor, *Deep-Sea Res. Part II Top. Stud. Oceanogr.*, 48, 3841–3868,
 601 2001.
- 602 Boetius, A., and Haeckel, M.: Mind the seafloor, *Science*, 359, 34–36,
 603 doi:10.1126/science.aap7301, 2018.
- 604 Boetius, A.: RV Sonne Fahrtbericht / Cruise Report SO242-2: JPI OCEANS Ecological
 605 Aspects of Deep-Sea Mining, DISCOL Revisited, Guayaquil-Guayaquil (Ecuador), 28.08.-
 606 01.10.2015, Kiel: Helmholtz-Zentrum für Ozeanforschung, 2015.
- 607 Borowski, C.: Physically disturbed deep-sea macrofaunal impacts of a large-scale physical
 608 disturbance experiment in the Southeast Pacific, *Deep-Sea Res. Part II Top. Stud.*
 609 *Oceanogr.*, 48, 3809–3839, 2001.
- 610 Borowski, C., and Thiel, H.: Deep-Sea macrofaunal impacts of a large-scale physical
 611 disturbance experiment in the Southeast Pacific, *Deep-Sea Res. Part II Top. Stud.*
 612 *Oceanogr.*, 45, 55–81, 1998.
- 613 Boudreau, B. P.: A one-dimensional model for bed-boundary layer particle exchange, *J. Mar.*
 614 *Syst.*, 11, 279–303, doi:10.1016/S0924-7963(96)00127-3, 1997.
- 615 Brenke, N.: An Epibenthic sledge for operations on marine soft bottom and bedrock, *J. Mar.*
 616 *Tech. Soc.*, 39, 10–19, 2005.
- 617 Brockett, T., and Richards, C. Z.: Deep-sea mining simulator for environmental impact studies,
 618 *Sea Technol.*, 35, 77–82, 1994.
- 619 Chung, J. S.: Full-Scale, Coupled Ship and Pipe Motions Measured in North Pacific Ocean:
 620 The Hughes Glomar Explorer with a 5,000-m-Long Heavy-Lift Pipe Deployed, *Proc. 19th*
 621 *ISOPE*, 20, 1–6, 2010.
- 622 Cronan, D. S., Rothwell, G., and Croudace, I.: An ITRAX geochemical study of
 623 ferromanganiferous sediments from the Penrhyn basin, South Pacific Ocean, *Mar.*
 624 *Geosour. Geotechnol.*, 28, 207–221, doi:10.1080/1064119X.2010.483001, 2010.
- 625 Cuvelier, D., Gollner, S., Jones, D. O. B., Kaiser, S., Arbizu, P. M., Menzel, L., Mestre, N. C.,
 626 Morato, T., Pham, C., Pradillon, F., Purser, A., Raschka, U., Sarrazin, J., Simon-Lledó, E.,
 627 Stewart, I.M., Stuckas, H., Sweetman, A. K., and Colaço, A.: Potential Mitigation and
 628 Restoration Actions in Ecosystems Impacted by Seabed Mining, *Front. Mar. Sci.*, 5,
 629 doi:10.3389/fmars.2018.00467, 2018.
- 630 Davies, A. J., Roberts, J. M., and Hall-Spencer, J.: Preserving deep-sea natural heritage:
 631 emerging issues in offshore conservation and management, *Biol. Conserv.*, 138, 299–312,
 632 doi:10.1016/j.biocon.2007.05.011, 2007.
- 633 Dunlop, K. M., van Oevelen, D., Ruhl, H. A., Huffard, C. L., Kuhnz, L. A., and Smith, K. L.:
 634 Carbon cycling in the deep eastern North Pacific benthic food web: Investigating the effect
 635 of organic carbon input, *Limnol. Oceanogr.*, 61, 1956–1968,
 636 https://doi.org/10.1002/lno.10345, 2016.
- 637 Emerson, S., Fischer, K., Reimers, C. and Heggie, D.: Organic carbon dynamics and
 638 preservation in deep-sea sediments, *Deep-Sea Res.*, 32, 1–21, 1985.



- 639 Froelich, P. N., Klinkhammer, G. P., Bender, M. L., Luedke, L. A., Heath, G. R., Cullen, C.,
 640 Dauphin, P., Hammond, D., Hartmann, B., and Maynard, V.: Early oxidation of organic
 641 matter in pelagic sediments of the Eastern Equatorial Pacific, suboxic diagenesis, *Geochim.*
 642 *Cosmochim. Acta*, 43, 1075-1090, 1979.
- 643 Fukushima, T.: Overview "Japan Deep-Sea Impact Experiment = JET", ISOPE-M-95-008,
 644 ISOPE, 1995.
- 645 Gillard, B., Purkiani, K., Chatzievangelou, D., Vink, A., Iversen, M. H., and Thomsen, L.:
 646 Physical and hydrodynamic properties of deep sea mining-generated, abyssal sediment
 647 plumes in the Clarion Clipperton Fracture Zone (eastern-central Pacific), *Elem. Sci. Anth.*,
 648 7, 2019.
- 649 Gingele, F. X., and Kasten, S.: Solid-phase manganese in Southeast Atlantic sediments:
 650 implications for the paleoenvironment. *Mar. Geol.*, 121, 317-332, 1994.
- 651 Glasby, G. P.: Lessons Learned from Deep-Sea Mining. *Science*, 289, 551-553,
 652 doi:10.1126/science.289.5479.551, 2000.
- 653 Glover, A. G. and Smith, C. R.: The deep-sea floor ecosystem: current status and prospects of
 654 anthropogenic change by the year 2025, *Environ. Conserv.*, 30, 219-241, 2003.
- 655 Gollner, S., Kaiser, S., Menzel, L., Jones, D. O. B., Brown, A., Mestre, N. C., van Oevelen, D.,
 656 Menot, L., Colaço, A., Canals, M., Cuvelier, D., Durden, J. M., Gebruk, A., Eghe, G. A.,
 657 Haeckel, M., Marcon, Y., Mevenkamp, L., Morato, T., Pham, C. K., Purser, A., Sanchez-
 658 Vidal, A., Vanreusel, A., Vink, A., and Arbizu, P. M.: Resilience of benthic deep-sea fauna
 659 to mining activities, *Mar. Environ. Res.*, 129, 76-101,
 660 doi:10.1016/j.marenvres.2017.04.010, 2017.
- 661 Greinert, J.: RV Sonne Fahrtbericht / Cruise Report SO242-1: JPI OCEANS Ecological Aspects
 662 of Deep-Sea Mining, DISCOL Revisited, Guayaquil-Guayaquil (Ecuador), 28.07.-
 663 25.08.2015, Kiel: Helmholtz-Zentrum für Ozeanforschung, 2015.
- 664 Grupe, B., Becker, H. J., and Oebius, H. U.: Geotechnical and sedimentological investigations
 665 of deep-sea sediments from a manganese nodule field of the Peru Basin, *Deep. Res. Part II*
 666 *Top. Stud. Oceanogr.*, 48, 3593-3608, 2001.
- 667 Haeckel, M., König, I., Riech, V., Weber, M. E., and Suess, E.: Pore water profiles and
 668 numerical modelling of biogeochemical processes in Peru Basin deep-sea sediments, *Deep.*
 669 *Res. Part II Top. Stud. Oceanogr.*, 48, 3713-3736, doi:10.1016/S0967-0645(01)00064-9,
 670 2001.
- 671 Hauquier, F., Macheriotou, L., Bezerra, T. N., Eghe, G., Martínez Arbizu, P., and Vanreusel,
 672 A.: Geographic distribution of free-living marine nematodes in the Clarion-Clipperton
 673 Zone: implications for future deep-sea mining scenarios, *Biogeosciences Discuss.*,
 674 https://doi.org/10.5194/bg-2018-492, under review, 2018.
- 675 Halfar, J., and Fujita, R. M.: Precautionary management of deep-sea mining, *Mar. Pol.*, 26, 103-
 676 106, 2002.
- 677 Halkyard, J. E.: Technology for Mining Cobalt Rich Manganese Crusts from Seamounts, *Proc.*
 678 *OCEANS '85*, 352-274, 1985.
- 679 Halbach, P., Friedrich, G., and von Stackelberg, U. (Eds.): The manganese nodule belt of the
 680 Pacific Ocean, Enke, Stuttgart, 1988.
- 681 Hein, J. R., Mizell, K., Koschinsky, A., and Conrad, T. A.: Deep-ocean mineral deposits as a
 682 source of critical metals for high- and green-technology applications: comparison with
 683 land-based resources, *Ore Geol. Rev.*, 51, 1-14, 2013.
- 684 Hoagland, P., Beaulieu, S., Tivey, M. A., Eggert, R. G., German, C., Glowka, L., and Lin, J.:
 685 Deep-sea mining of seafloor massive sulfides, *Mar. Pol.*, 34, 728-732,
 686 doi:10.1016/j.marpol.2009.12.001, 2010.
- 687 International Seabed Authority (ISA): A Geological Model for Polymetallic Nodule Deposits
 688 in the Clarion-Clipperton Fracture Zone, Technical Study 6, Kingston, p. 211, 2010.



- 689 Jankowski, J. A., and Zielke, W.: The mesoscale sediment transport due to technical activities
 690 in the deep sea, *Deep. Res. Part II Top. Stud. Oceanogr.*, 48, 3487–3521, 2001.
- 691 Jones, D. O. B., Kaiser, S., Sweetman, A. K., Smith, C. R., Menot, L., Vink, A., Trueblood, D.,
 692 Greinert, J., Billett, D. S. M., Martínez Arbizu, P., Radziejewska, T., Singh, R., Ingle, B.,
 693 Stratmann, T., Simon-Lledó, E., Durden, J. M., and Clark, M. R.: Biological responses to
 694 disturbance from simulated deep-sea polymetallic nodule mining, *PLoS One*, 12,
 695 e0171750, <https://doi.org/10.1371/journal.pone.0171750>, 2017.
- 696 Juan, C., Van Rooij, D., and De Bruycker, W.: An assessment of bottom current controlled
 697 sedimentation in Pacific Ocean abyssal environments, *Mar. Geol.*, 403, 20–33, 2018.
- 698 Khripounoff, A., Caprais, J.-C., Crassous, P. and Etoubleau, J.: Geochemical and biological
 699 recovery of the disturbed seafloor in polymetallic nodule fields of the Clipperton-Clarion
 700 Fracture Zone (CCFZ) at 5,000-m depth, *Limnol. Oceanogr.*, 51, 2033–2041,
 701 doi:10.4319/lo.2006.51.5.2033, 2006.
- 702 König, I., Haeckel, M., Lougear, A., Suess, E., and Trautwein, A. X.: A geochemical model of
 703 the Peru Basin deep-sea floor - and the response of the system to technical impacts, *Deep.*
 704 *Res. Part II Top. Stud. Oceanogr.*, 48, 3737–3756, doi:10.1016/S0967-0645(01)00065-0,
 705 2001.
- 706 Kotlinski R., and Stoyanova V.: Physical, Chemical, and Geological changes of Marine
 707 Environment Caused by the Benthic Impact Experiment at the IOM BIE Site, *Proc. 8th*
 708 *ISOPE 2*, 277–281, Montreal, Canada, 1998.
- 709 Kretschmer, S., Geibert, W., Rutgers van der Loeff, M. M., and Mollenhauer, G.: Grain size
 710 effects on 230Thxs inventories in opal-rich and carbonate-rich marine sediments, *Earth*
 711 *Planet. Sci. Lett.*, 294, 131–142, doi:10.1016/j.epsl.2010.03.021, 2010.
- 712 Kuhn, G.: Don't forget the salty soup: Calculations for bulk marine geochemistry and
 713 radionuclide geochronology, *Goldschmidt 2013 Florence, Italy*, 25 August 2013 - 30
 714 August 2013, doi:10.1180/minmag.2013.077.5.11, 2013.
- 715 Kuhn, T., Wegorzewski, A. V., Rühlemann, C., and Vink, A.: Composition, formation, and
 716 occurrence of polymetallic nodules, in: *Deep-Sea Mining*, edited by: Sharma, R., 23–63,
 717 Springer International Publishing, Cham., doi:10.1007/978-3-319-52557-0_2, 2017a.
- 718 Kuhn, T., Versteegh, G. J. M., Villinger, H., Dohrmann, I., Heller, C., Koschinsky, A., Kaul,
 719 N., Ritter, S., Wegorzewski, A. V. and Kasten, S.: Widespread seawater circulation in 18–
 720 22 Ma oceanic crust: Impact on heat flow and sediment geochemistry, *Geology*, 45, 799–
 721 802, doi:10.1130/G39091.1, 2017b.
- 722 Kuhn, T., Rühlemann, C., and Wiedicke-Hombach, M.: Developing a strategy for the
 723 exploration of vast seafloor areas for prospective manganese nodule fields, in: *Marine*
 724 *Minerals: Finding the Right Balance of Sustainable Development and Environmental*
 725 *Protection*, edited by Zhou, H., and Morgan, C. L., The Underwater Mining Institute,
 726 Gelendzhik, Russia (K 1-12), 2012.
- 727 Lodge, M., Johnson, D., Le Gurun, G., Wengler, M., Weaver, P., and Gunn, V.: Seabed mining:
 728 International Seabed Authority environmental management plan for the Clarion–
 729 Clipperton Zone. A partnership approach, *Mar. Pol.*, 49, 66–72,
 730 doi:10.1016/j.marpol.2014.04.006, 2014.
- 731 Madureira, P., Brekke, H., Cherkashov, G., and Rovere, M.: Exploration of polymetallic
 732 nodules in the Area: Reporting practices, data management and transparency, *Mar. Pol.*,
 733 70, 101–107, doi:10.1016/j.marpol.2016.04.051, 2016.
- 734 Martínez Arbizu, P., and Haeckel, M.: RV SONNE Fahrtbericht / Cruise Report SO239:
 735 EcoResponse Assessing the Ecology, Connectivity and Resilience of Polymetallic Nodule
 736 Field Systems, Balboa (Panama) – Manzanillo (Mexico,) 11.03.-30.04.2015 (Report No.
 737 doi:10.3289/GEOMAR_REP_NS_25_2015), GEOMAR Helmholtz-Zentrum für
 738 Ozeanforschung, Kiel, Germany, 2015.



- Menendez, A., James, R. H., Lichtschlag, A., Connelly, D. and Peel, K.: Controls on the chemical composition on ferromanganese nodules in the Clarion-Clipperton Fracture Zone, eastern equatorial Pacific, *Mar. Geol.*, 409, 1-14, 2018.
- Menot, L., and Rühlemann, C., and BIONOD Shipboard party: BIONOD Cruise Science Report, Vol. 2 French Licence Area, Ifremer, REM/EEP/LEP13.06, 57p, 2013.
- Mero, J. L.: *The Mineral Resources of the Sea*, Elsevier, Amsterdam, 1965.
- Mewes, K., Mogollón, J. M., Picard, A., Rühlemann, C., Eisenhauer, A., Kuhn, T., Ziebis, W., and Kasten, S.: Diffusive transfer of oxygen from seamount basaltic crust into overlying sediments: An example from the Clarion-Clipperton Fracture Zone, *Earth Planet. Sci. Lett.*, 433, 215–225, doi:10.1016/j.epsl.2015.10.028, 2016.
- Mewes, K., Mogollón, J. M., Picard, A., Rühlemann, C., Kuhn, T., Nöthen, K., and Kasten, S.: Impact of depositional and biogeochemical processes on small scale variations in nodule abundance in the Clarion-Clipperton Fracture Zone, *Deep-Sea Res. Part I: Oceanogr. Res. Pap.*, 91, 125–141, doi:10.1016/j.dsr.2014.06.001, 2014.
- Miljutin, D. M., Miljutina, M. A., Martínez Arbizu, P., and Galeron, J.: Deep-sea nematode assemblage has not recovered 26 years after experimental mining of polymetallic nodules (CCFZ, Pacific), *Deep-Sea Res. Part I: Oceanogr. Res. Pap.*, 58, 885–897, 2011.
- Mogollón, J. M., Mewes, K., and Kasten, S.: Quantifying manganese and nitrogen cycle coupling in manganese-rich, organic carbon-starved marine sediments: Examples from the Clarion-Clipperton fracture zone, *Geophys. Res. Lett.*, 43, 2016GL069117, doi:10.1002/2016GL069117, 2016.
- Morgan, C. L., Nichols, J. A., Selk, B. W., Toth, J. R., and Wallin, C.: Preliminary analysis of exploration data from Pacific deposits of manganese nodules, *Mar. Georesour. Geotechnol.*, 11, 1-25, 1993.
- Müller, P. J., Hartmann, M., and Suess, E.: The chemical environment of pelagic sediments, in: *The Manganese Nodule Belt of the Pacific Ocean: Geological Environment, Nodule Formation, and Mining Aspects*, edited by Halbach, P., Friedrich, G., and von Stackelberg, U., Enke, Stuttgart, pp. 70-90, 1988.
- Müller, P. J., and Mangini, A.: Organic carbon decomposition rates in sediments of the Pacific manganese nodule belt dated by ²³⁰Th and ²³¹Pa, *Earth Planet. Sci. Lett.*, 51, 94-114, 1980.
- Nöthen, K., and Kasten, S.: Reconstructing changes in seep activity by means of pore water and solid phase Sr/Ca and Mg/Ca ratios in pockmark sediments of the Northern Congo Fan, *Mar. Geol.*, 287, 1–13, doi:10.1016/j.margeo.2011.06.008, 2011.
- Oebius, H. U., Becker, H. J., Rolinski, S., and Jankowski, J. A.: Parametrization and evaluation of marine environmental impacts produced by deep-sea manganese nodule mining, *Deep-Sea Res. Part II Top. Stud. Oceanogr.*, 48, 3453–3467, doi:10.1016/S0967-0645(01)00052-2, 2001.
- Paul, S. A. L., Gaye, B., Haeckel, M., Kasten, S., and Koschinsky, A.: Biogeochemical Regeneration of a Nodule Mining Disturbance Site: Trace Metals, DOC and Amino Acids in Deep-Sea Sediments and Pore Waters, *Front. Mar. Sci.*, 5, doi:10.3389/fmars.2018.00117, 2018.
- Pearson, K.: Notes on regression and inheritance in the case of two parents, *Proc. Royal Soc. London*, 58, 240–242, 1895.
- Purser, A., Marcon, Y., Hoving, H.-J. T., Vecchione, M., Piatkowski, U., Eason, D., Bluhm, H., and Boetius, A.: Association of deep-sea incirrate octopods with manganese crusts and nodule fields in the Pacific Ocean, *Curr. Biol.*, 26, R1268–R1269, doi:10.1016/j.cub.2016.10.052, 2016, 2016.
- Radziejewska, T.: Response of deep-sea meiobenthic communities to sediment disturbance simulating effects of polymetallic nodule mining, *Int. Rev. Hydrobiol.*, 87, 457-477, 2002.



- Ramirez-Llodra E., Tyler P. A., Baker M. C., Bergstad O. A., Clark M. R., Escobar, E., Levin, L. A., Menot, L., Rowden, A. A., Smith, C. R., and Van Dover, C. L.: Man and the Last Great Wilderness: Human Impact on the Deep Sea, PLoS ONE, 6, e22588, doi:10.1371/journal.pone.0022588, 2011.
- Redfield, A. C.: On the proportions of organic derivations in sea water and their relation to the composition of plankton, in: James Johnstone Memorial Volume, edited by Daniel, R. J., University Press of Liverpool, pp. 176–192, 1934.
- Rühlemann, C., Kuhn, T., Wiedicke, M., Kasten, S., Mewes, K., and Picard, A.: Current status of manganese nodule exploration in the German license area, Proceedings of the Ninth (2911) ISOPE Ocean Mining Symposium, Maui, Hawaii, USA, June 19-24, 2011, 168-173, 2011.
- Rühlemann, C., Albers, L., Briand, P., Brulport, J.-P., Cosson, R., Dekov, V. M., Galéron, J., Goergens, R., Gueguen, B., Hansen, J., Kaiser, S., Kefel, O., Khripounoff, A., Kuhn, T., Larsen, K., Menot, L., Mewes, K., Miljutin, D., Mohrbeck, I., Nealova, L., Perret-Gentil, L., Regocheva, A., Węgorzewski, A., and Zoch, D., BIONOD Cruise report, p. 299, 2012.
- Scott, S. D.: Seafloor Polymetallic Sulfides: Scientific Curiosities or Mines of the Future? In: Marine Minerals, edited by: Teleki, P. G., Dobson, M. R., Moore, J. R., and von Stackelberg, U., NATO ASI Series (Series C: Mathematical and Physical Sciences), 194, Springer, Dordrecht, 1987.
- Sharma, R.: Indian Deep-sea Environment Experiment (INDEX):: An appraisal. Deep-Sea Res. Part II Top. Stud. Oceanogr., 48, 3295-3307, doi:10.1016/S0967-0645(01)00041-8, 2001.
- Smith, C. R., Levin, L. A., Koslow, A., Tyler, P. A., and Glover, A. G.: The near future of the deep seafloor ecosystems, in: Aquatic Ecosystems: Trends and Global Prospects, edited by Polunin, N. V. C., Cambridge University Press, 334–353, doi:10.1017/CBO9780511751790.030, 2008.
- Smith, K. L., White, G. A., and Laver, M. B.: Oxygen uptake and nutrient exchange of sediments measured in situ using a free vehicle grab respirometer. Deep Sea Res. Part II, 26, 337-346, doi:10.1016/0198-0149(79)90030-X, 1979.
- Soetaert, K., and Meysman, F.: Reactive transport in aquatic ecosystems: Rapid model prototyping in the open source software R, Environ. Model. Softw., 32, 49–60, doi:10.1016/j.envsoft.2011.08.011, 2012.
- Spickermann, R.: Rare Earth Content of Manganese Nodules in the Lockheed Martin Clarion-Clipperton Zone Exploration Areas, Proc. Off. Technol. Conf., Houston Texas, 2012.
- Stratmann, T., Lins, L., Purser, A., Marcon, Y., Rodrigues, C. F., Ravara, A., Cunha, M. R., Simon-Lledó, E., Jones, D. O. B., Sweetman, A. K., Köser, K., and van Oevelen, D.: Abyssal plain faunal carbon flows remain depressed 26 years after a simulated deep-sea mining disturbance, Biogeosciences, 15, 4131-4145, doi.org/10.5194/bg-15-4131-2018, 2018.
- Thiel, H., and Forschungsverband Tiefsee-Umweltschutz: Evaluation of the environmental consequences of polymetallic nodule mining based on the results of the TUSCH Research Association, Deep-Sea Res. Part II Top. Stud. Oceanogr., 48, 3433-3452, doi:10.1016/S0967-0645(01)00051-0, 2001.
- Trueblood, D. D., and Ozturgut, E.: The benthic impact experiment: A study of the ecological impacts of deep seabed mining on abyssal benthic communities, Proc. of the 7th ISOPE Conference, Honolulu, Hawaii, 1997.
- Van Dover, C. L.: Tighten regulations on deep-sea mining, Nature, 470, 31-33, doi:10.1038/470031a, 2011.
- Vanreusel, A., Hilario, A., Ribeiro, P. A., Menot, L., and Arbizu, P. M.: Threatened by mining, polymetallic nodules are required to preserve abyssal epifauna, Sci. Rep., 6, 26808, doi:10.1038/srep26808, 2016.



- 839 Volz, J. B., Liu, B., Köster, M., Henkel, S., Koschinsky, A., and Kasten, S.: Post-depositional
 840 manganese mobilization during the last glacial period in sediments of the eastern Clarion-
 841 Clipperton Zone, Pacific Ocean, *Earth Planet. Sci. Lett.*, under review.
- 842 Volz, J. B., Mogollón, J. M., Geibert, W., Martínez Arbizu, P., Koschinsky, A., Kasten, S.:
 843 Natural spatial variability of depositional conditions, biogeochemical processes and
 844 element fluxes in sediments of the eastern Clarion-Clipperton Zone, Pacific Ocean, *Deep-*
 845 *Sea Res. Part I*, 140, 159-172, 2018.
- 846 Wedding, L. M., Reiter, S. M., Smith, C. R., Gjerde, K. M., Kittinger, J. N., Friedlander, A. M.,
 847 Gaines, S. D., Clark, M. R., Thurnherr, A. M., Hardy, S. M., and Crowder, L. B.: Managing
 848 mining of the deep seabed, *Science*, 349, 144-145, 2015.
- 849 Widmann, P.: Enrichment of mobilizable manganese in relation to manganese nodules
 850 abundance, Master thesis, Eberhard Karls Universität Tübingen and the Federal Institute for
 851 Geoscience and Resources, Hannover, 182 p., 2015.
- 852 Ziebis, W., McManus, J., Ferdelman, T., Schmidt-Schierhorn, F., Bach, W., Muratli, J.,
 853 Edwards, K. J., and Villinger, H.: Interstitial fluid chemistry of sediments underlying the
 854 North Atlantic gyre and the influence of subsurface fluid flow, *Earth Planet. Sci. Lett.*,
 855 323–324, 79–91, doi:10.1016/j.epsl.2012.01.018, 2012.
- 856 Zonneveld, K., Versteegh, G., Kasten, S., Eglinton, T. I., Emeis, K.-C., Huguët, C., Koch, B.
 857 P., de Lange, G. J., de Leeuw, J. W., Middelburg, J. J., Mollenhauer, G., Prahl, F.,
 858 Rethemeyer, J. and Wakeham, S.: Selective preservation of organic matter in marine
 859 environments; processes and impact on the sedimentary record, *Biogeosciences*, 7, 483-
 860 511, 2010.
- 861
- 862



863 **Figure captions**

864 Figure 1: Sampling sites (black circles, black star) in various European contract areas for the
 865 exploration of manganese nodules within the Clarion-Clipperton Fracture Zone (CCZ).
 866 Investigated stations are located in the German BGR area (blue), eastern European IOM area
 867 (yellow), Belgian GSR area (green) and French IFREMÉR area (red). The two stations within
 868 the German BGR area are located in the “prospective area” (BGR-PA, black star) and in the
 869 “reference area” (BGR-RA, black circle). The contract areas granted by the International
 870 Seabed Authority (ISA) are surrounded by nine Areas of Particular Environmental Interest
 871 (APEI), which are excluded from any mining activities (green shaded squares). Geographical
 872 data provided by the ISA.

873 Figure 2: Examples of undisturbed reference sediments in the German BGR-PA area and the
 874 French IFREMÉR area and pictures of small-scale disturbances for the simulation of deep-sea
 875 mining within the CCZ, which are investigated in the framework of this study (years: yr;
 876 months: mth; days: d). Copyright: ROV KIEL 6000 Team, GEOMAR Helmholtz Centre for
 877 Ocean Research Kiel, Germany.

878 Figure 3: Solid-phase Mn and TOC contents for all disturbed sites investigated in the framework
 879 of this study.

880 Figure 4: Correlation of solid-phase Mn and TOC contents between the disturbed sites and the
 881 respective undisturbed reference sediments (grey shaded profiles) using the disturbance depths
 882 determined with the Pearson correlation coefficient (compare Table 3). For the undisturbed
 883 reference sediments, solid-phase Mn contents are taken from Volz et al. (under review) and
 884 TOC contents are taken from Volz et al. (2018).

885 Figure 5: Model results of the transient transport-reaction model for (a) EBS disturbance in the
 886 German BGR-RA area and (b) the IOM-BIE disturbance in the eastern European IOM area.

887 Figure 6: Detailed model results of the transient transport-reaction model for the upper 1 m of
 888 the sediments for (a) EBS disturbance in the German BGR-RA area and (b) the IOM-BIE
 889 disturbance in the eastern European IOM area.

890 Figure 7: Pore-water fluxes of oxygen (O_2), nitrate (NO_3^{2-}) and ammonia (NH_4^+) at the
 891 sediment-water interface obtained by the application of the transient transport-reaction model.
 892 Oxygen fluxes into the sediment and fluxes of nitrate and ammonia towards the sediment
 893 surface are shown as a function of time after the EBS and IOM-BIE disturbances in the German
 894 BGR-RA area (blue) and in the eastern European IOM area (black), respectively.

895 Figure 8: Conceptual model for time-dependent pore-water fluxes of oxygen (O_2), nitrate
 896 (NO_3^{2-}) and ammonia (NH_4^+) at the sediment-water interface after the removal of the upper 7-
 897 10 cm of the sediments. The re-establishment of bioturbation, the maximum oxygen penetration
 898 depth (OPD) as well as the re-establishment of the surface sediment layer dominated by the
 899 reactive labile organic matter fraction are indicated as a function of time after the sediment
 900 removal.



901 **Table captions**

902 Table 1: MUC and PC cores investigated in this study including information on geographic
903 position, water depth, type and age of the disturbances (years: yr; months: mth; days: d).

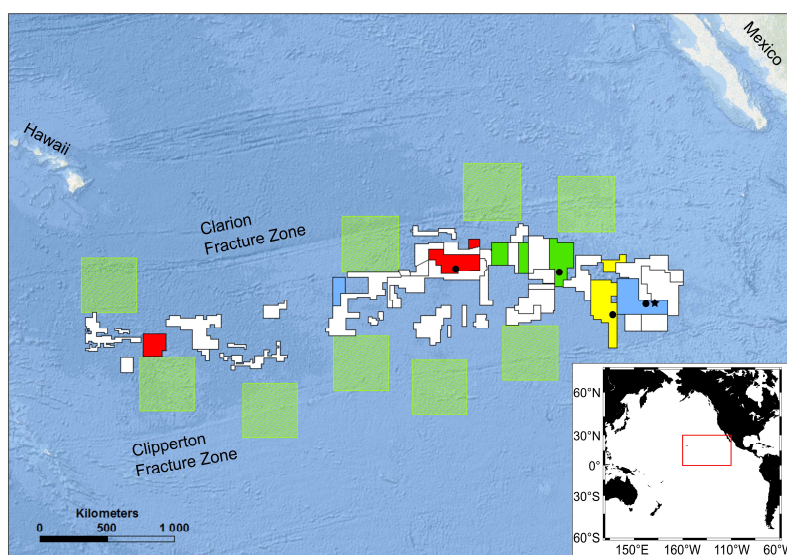
904 Table 2: Information of sedimentation rate (Sed. rate), flux of particulate organic carbon (POC)
905 to the seafloor, bioturbation depth (Bioturb. depth), oxygen penetration depth (OPD) based on
906 GC cores from the investigated sites and determined in the study by Volz et al. (2018).
907 Information for the BGR-PA area is taken from an adjacent site (A5-2-SN; 11°57.22'N,
908 117°0.42'W) studied by Mewes et al. (2014) and Mogollón et al. (2016).

909 Table 3: Calculated Pearson correlation coefficients r_{Mn} and r_{TOC} for the determination of the
910 disturbance depth of various small-scale disturbances investigated in the framework of this
911 study (compare Table 1).

912



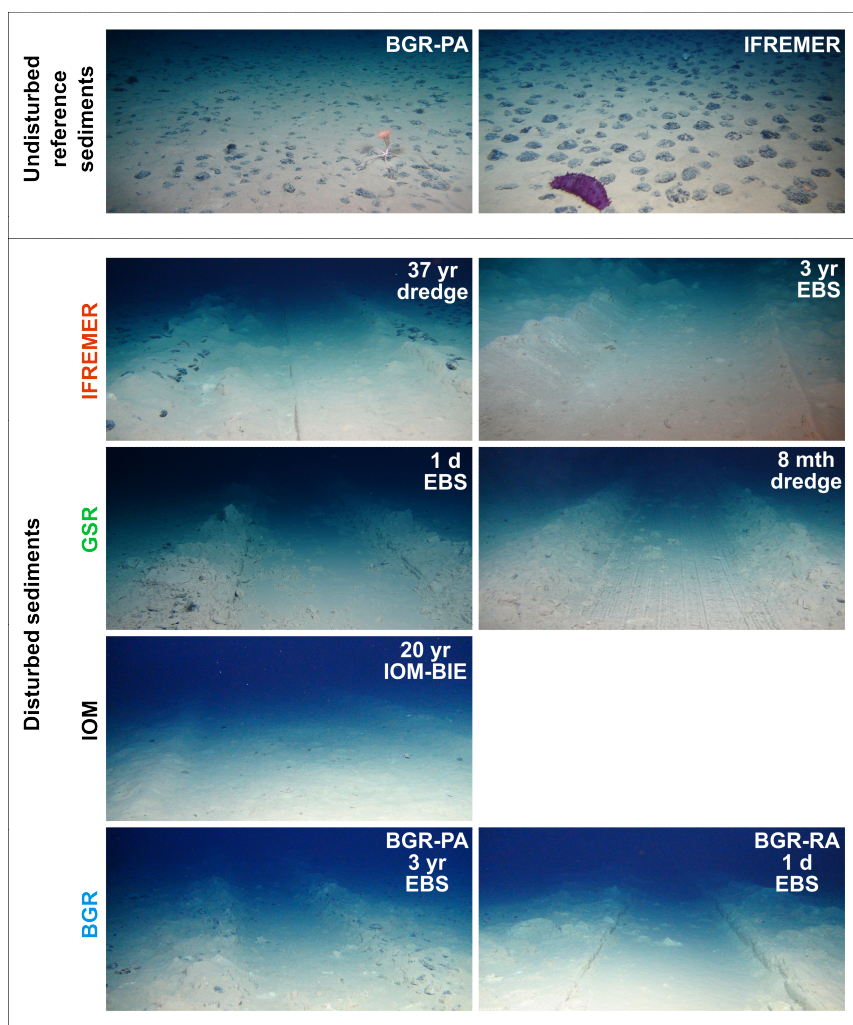
913 **Figure 1:**



914
 915
 916



917 **Figure 2:**

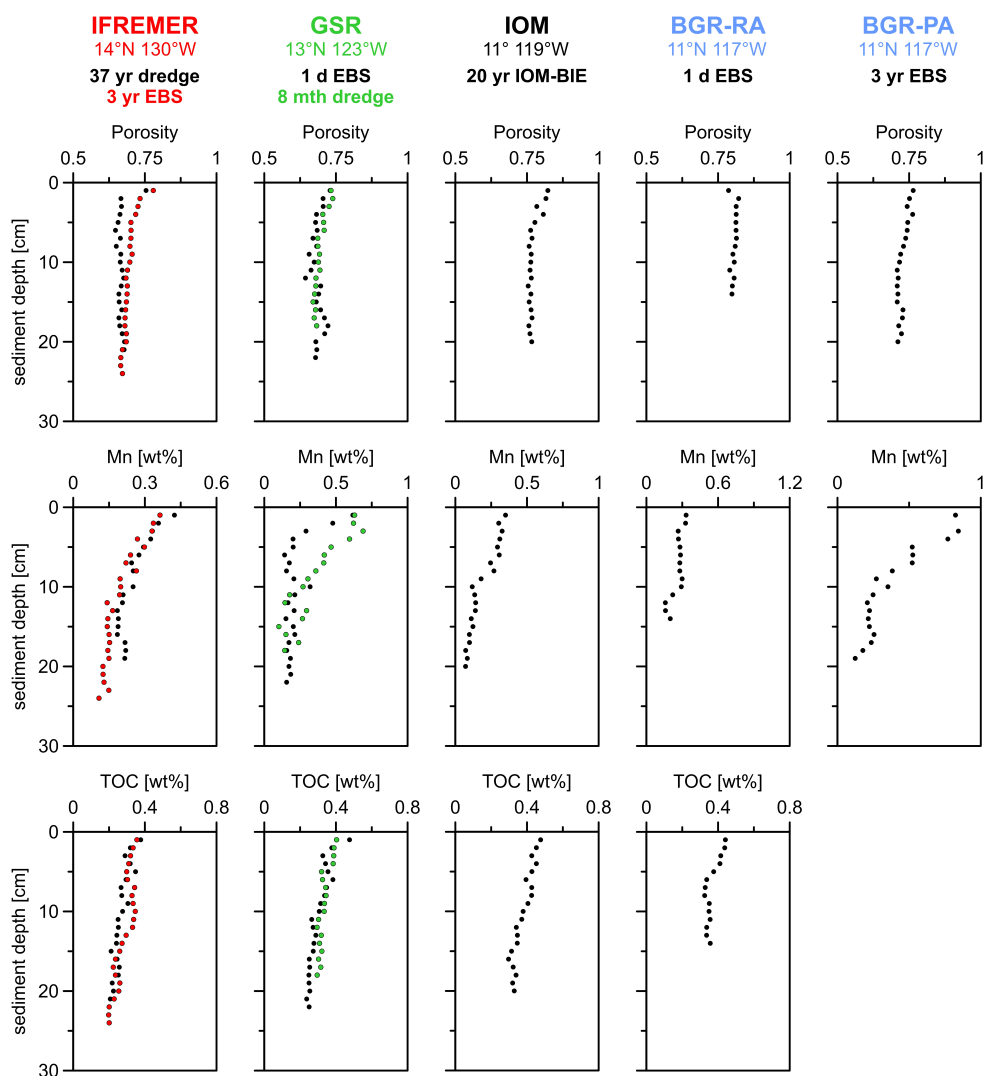


918
 919

920



921 **Figure 3:**

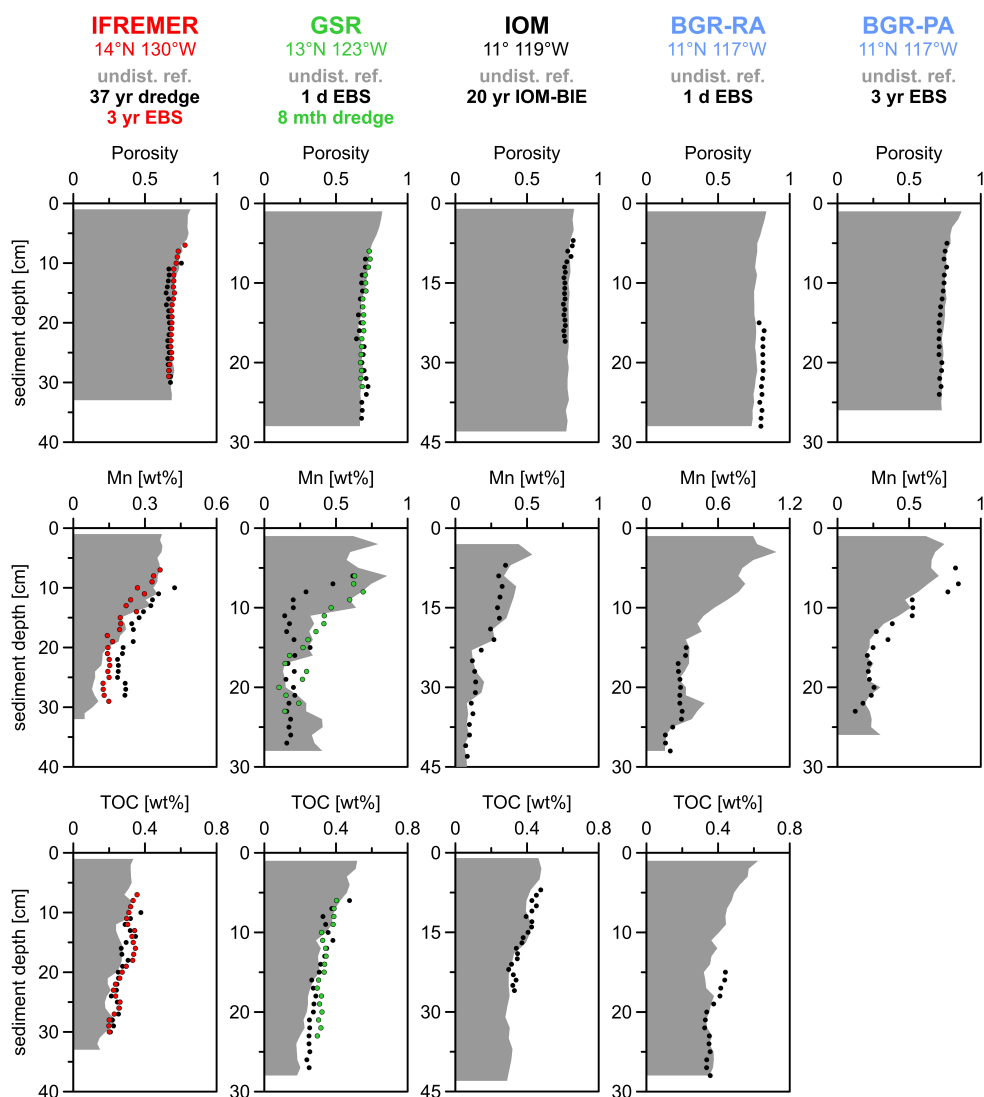


922

923



924 **Figure 4:**

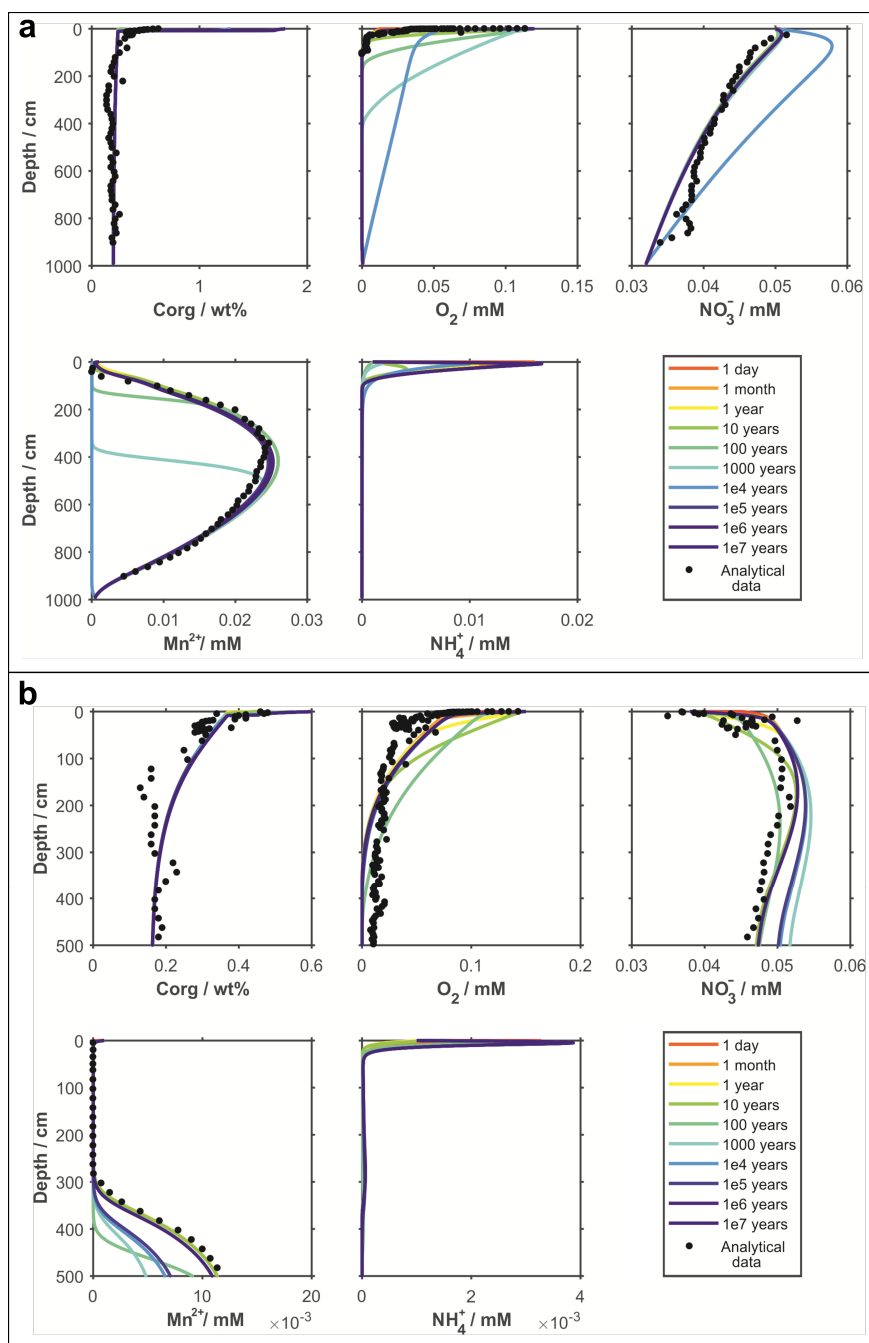


925

926



927 **Figure 5:**

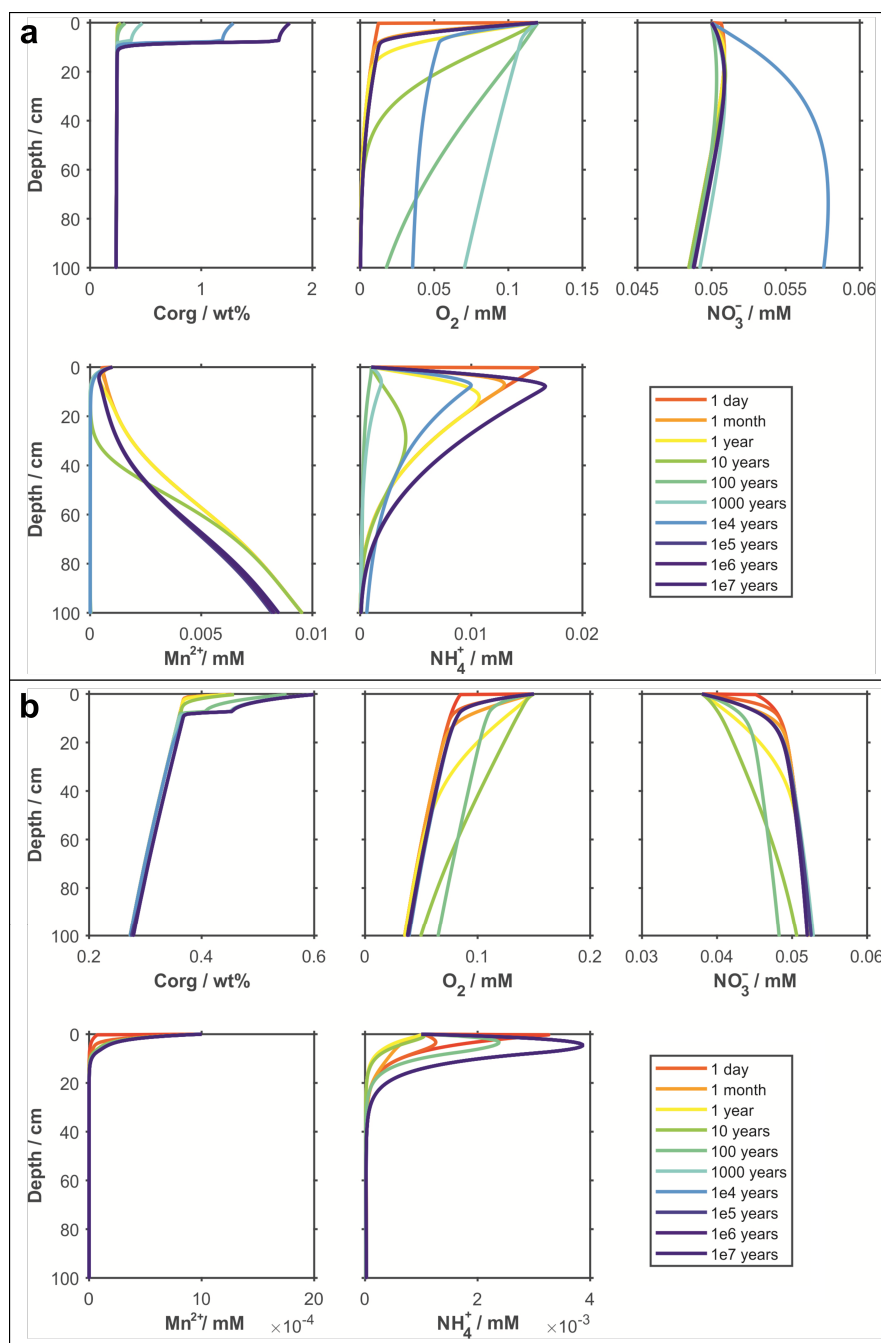


928

929



930 **Figure 6:**

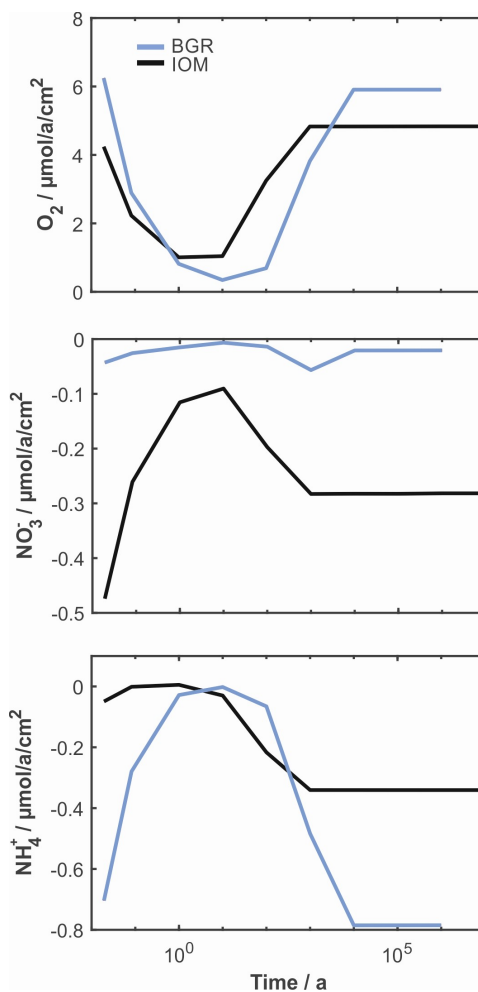


931

932



933 **Figure 7:**



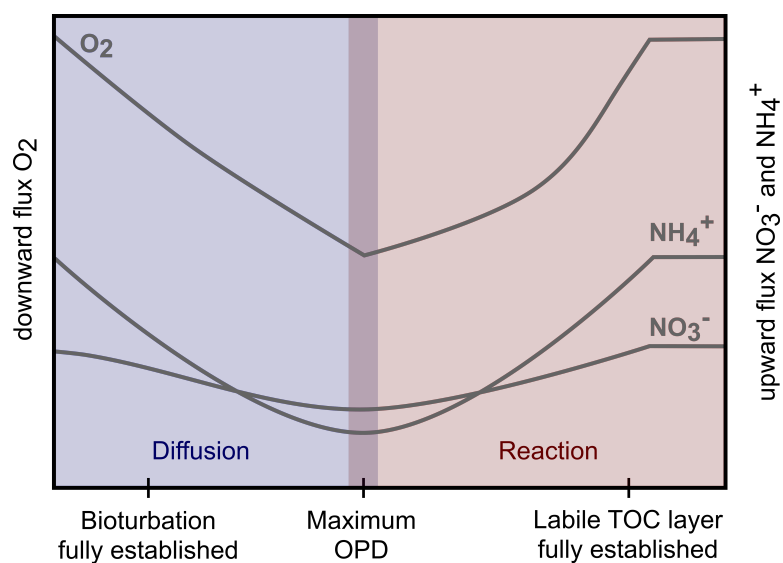
934

935

936



937 **Figure 8:**



938

939



940 **Table 1:**

Area	Site	Coring device	Disturbance device/type	Disturbance age	Latitude [N]	Longitude [W]	Water depth [m]
BGR-PA	39	MUC	-	-	11°50.64'	117°03.44'	4132.0
BGR-PA	41	PC	EBS ¹	3 yr	11°50.92'	117°03.77'	4099.2
BGR-RA	62	GC	-	-	11°49.12'	117°33.22'	4312.2
BGR-RA	64	PC	EBS ²	1 d	11°48.27'	117°30.18'	4332
BGR-RA	66	MUC	-	-	11°49.13'	117°33.13'	4314.8
IOM	84	MUC	-	-	11°04.73'	119°39.48'	4430.8
IOM	87	GC	-	-	11°04.54'	119°39.83'	4436
IOM	101	PC	IOM-BIE ³	20 yr	11°04.38'	119°39.38'	4387.4
GSR	121	MUC	-	-	13°51.25'	123°15.3'	4517.7
GSR	131	PC	EBS ²	1 d	13°52.38'	123°15.1'	4477.6
GSR	141	PC	dredge ⁴	8 mth	13°51.95'	123°15.33'	4477
IFREMER	157	PC	dredge ⁵	37 yr	14°02.06'	130°07.23'	4944.5
IFREMER	161	PC	EBS ¹	3 yr	14°02.20'	130°05.87'	4999.1
IFREMER	175	MUC	-	-	14°02.45'	130°05.11'	5005.5

941 ¹Epibenthic sledge (EBS) during BIONOD cruises in 2012 onboard L'Atalante (Brenke, 2005; Rühlemann and
 942 Menot, 2012; Menot and Rühlemann, 2013)

943 ²Epibenthic sledge (EBS) during RV SONNE cruise SO239 in 2015 (Brenke, 2005; Martínez Arbizu and
 944 Haeckel, 2015)

945 ³Benthic impact experiment (BIE); disturbance created with the Deep-Sea Sediment Re-suspension System
 946 (DSSRS; e.g., Brockett and Richards, 1994; Kotlinski et al., 1998)

947 ⁴Towed dredge sampling during GSR cruise in 2014 onboard M.V. Mt Mitchell (Jones et al., 2017)

948 ⁵Towed dredge sampling by the Ocean Minerals Company (OMCO) in 1978 onboard Hughes Glomar Explorer
 949 (Morgan et al., 1993; Spickermann, 2012)

950



951 **Table 2:**

Area	Sed. rate [cm kyr ⁻¹]	POC flux [mg m ⁻² d ⁻¹]	Bioturb. depth [cm]	OPD [m]
BGR-PA	~0.53 ^a	~6.9 ^a	~5 ^a	~2 ^{a,b}
BGR-RA	0.65	1.99	7	0.5
IOM	1.15	1.54	13	3
GSR	0.21	1.51	8	>7.4
IFRE-1	0.64	1.47	7	4.5
IFRE-2	0.48	1.5	8	3.8
APEI3	0.2	1.07	6	>5.7

952 ^aMogollón et al. (2016)

953 ^bMewes et al. (2014)

954

955



956 **Table 3:**

Exploration area	Disturbance device/type	Disturbed Site	Reference Site	r_{Mn}	Disturbance depth [cm]	r_{TOC}
BGR-PA	EBS	41	39	0.86	5	-
BGR-RA	EBS	64	66	0.82	15	-0.4
IOM	IOM-BIE	101	87	0.97	7	0.77
GSR	EBS	131	121	0.72	6	0.88
GSR	dredge	141	121	0.88	6	0.91
IFREMER	dredge	157	175	0.74	10	0.73
IFREMER	EBS	161	175	0.93	7	0.74

957

958